Modeling the Structure and Spectroscopy of Alkaline Zeolites

Karl D. Hammond[1] and Scott M. Auerbach[1,2,1]

[1]Department of Chemical Engineering and [2]Department of Chemistry
University of Massachusetts Amherst, Amherst, MA 01003

Running title: Modeling Basic Zeolites

ABSTRACT

We review recent efforts at modeling the structure and spectroscopy of basic zeolites and related microporous oxides. We restrict our attention to materials with enhanced basicity through framework substitution of oxygen atoms in Si–O–Si linkages with NH groups, yielding "nitrided" Si–NH–Si structures. We also consider such nitridation in alumino-silicates, alumino-phosphates and other related solids. We briefly review the synthetic literature claiming to have made such nitrided materials, and discuss efforts at characterizing these zeolites. We note a paucity of unambiguous evidence pointing to nitrogen substitution into intact frameworks. We suggest that modeling vibrational and magnetic spectroscopies may yield such evidence. We discuss *ab initio* and density functional theory methods for computing infrared, Raman, and nuclear magnetic resonance spectra, with a focus on challenges that arise when modeling zeolites and related solids. We review recent efforts at modeling the structure, spectroscopy, and catalytic activity of nitrided zeolites. We suggest that recent modeling, in collaboration with experiments, has established the existence of nitrogen in zeolite frameworks, but that more work is necessary to determine the stabilities and optimal applications of nitrided zeolites as catalysts.

[1] Corresponding author; email: auerbach@chem.umass.edu.

1. INTRODUCTION

Zeolites acting as acid catalysts have replaced homogeneous acid catalysts in many chemical processes. Strong Brønsted–Lowry acidity and sub-nanometer pores in zeolites provide a unique combination of high catalytic activity, strong acidity, selective reaction, and relative ease of separation [1]. There is a significant fraction of industrially important reactions that are catalyzed by *bases* [2], however, and the strongly acidic nature of zeolites means their conjugate bases are relatively weak if not neutral. There has been interest in the last fifty years [3]—particularly in the last ten—in preparing zeolites that act as strong bases, both by synthetic and post-synthetic routes.

Strongly basic zeolites offer the same promise of selectivity, ease of separation, and high activity for reactions that either require base catalysts or in which the resulting chemistry is different when a base catalyst (as opposed to an acid) is used. Applications of base catalysis using zeolites prior to 2001 have been reviewed by Weitkamp [4] and Barthomeuf [5]. These applications have become even more important in recent years due to the surge of interest in biomass conversion reactions, many of which require base catalysts or are more active with alkaline catalysts than with acids [6,7].

There are three primary methods of making zeolites and related materials behave as bases:

1. Ion exchange of sodium or ammonium ions for calcium, magnesium, rubidium, cesium, or barium ions [2];
2. Grafting organic bases onto the pore walls, particularly in mesoporous materials [4,8–10];
3. Substitution of nitrogen for oxygen (or, similarly, substitution of oxygen for nitrogen in silicon nitride).

Ion exchange methods aim to increase Lewis base strengths by replacing the charge-compensating cation with an ion that increases the electron density on the oxygen atoms in the framework. Such ion-exchanged zeolites are often too weak to serve as active catalysts [11].

Grafting methods simply take a strong base and attach it to a porous material. This has the effect of turning the porous material into a catalytic support. Grafts have the unfortunate problem of decreasing the effective pore diameter, and are therefore typically

limited to materials with large pore diameters such as SBA-15, MCM-41, and MCM-48. The larger numbers of Si–OH surface defects in amorphous mesoporous materials also provide more anchoring points for grafted bases than are available in zeolites.

Substitution of oxygen for nitrogen in a silicate is analogous to the difference between an ether and a secondary amine in organic compounds: ethers are typically neutral, whereas amines are much stronger bases. The distinct advantage of nitrogen substitution is that the substitution is of the form Si–O–Si → Si–NH–Si or Si–OH–Al → Si–NH_2–Al, which, in principle, leaves the size of the zeolite pores virtually unchanged. In practice, however, such "nitridation" often competes with dealumination and decomposition reactions, which can render the resulting material riddled with defects and even non-porous. In addition, the exact nature of where and how the substitution process occurs remains mysterious, with characterization methods hinting at but not really proving the existence of nitrogen in zeolite frameworks. As such, there is much to be learned from both modeling and spectroscopy of these intriguing materials, especially regarding the nature of basic sites in nitrided zeolites, and the framework structures that result.

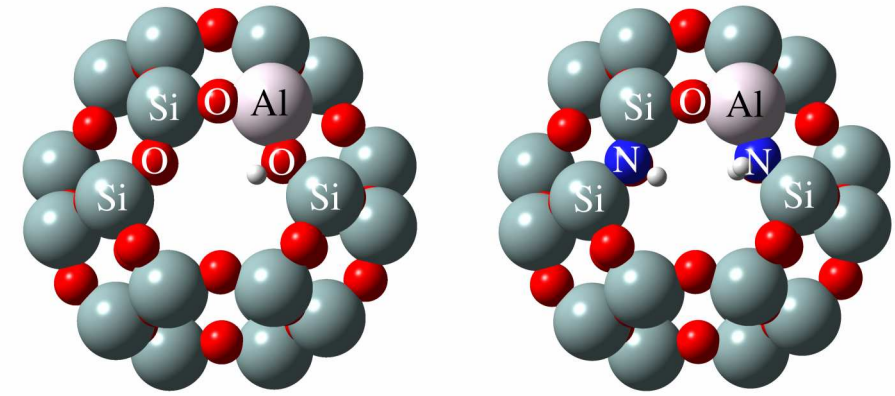

Figure 1. Sodalite cage showing an unsubstituted cage with an acid site (left) and the same cage with two nitrogen substitutions, one forming an Si–NH–Si group and another forming an Si–NH_2–Al group (right).

The rest of this chapter is intended to provide an overview of synthesis and characterization procedures that have been used to produce nitrogen-substituted zeolites for use in base catalysis, with a strong emphasis on characterization via simulation of structural properties as well as infrared and nuclear magnetic resonance (NMR) spectroscopy.

2. NITROGEN-SUBSTITUTED SILICATES

Nitrogen-substituted zeolites, amorphous silicates, and aluminophosphates are typically prepared by high-temperature treatment of the starting material with ammonia or another amine. High temperatures—as high as 1000°C in the case of some mesoporous materials [12]—seem to be required to break Si–O bonds. For zeolites, temperatures of 800–850°C are common [13,14]. Care must be taken to ensure complete removal of water from the vicinity of the zeolite surface after the reaction, or dealumination may result instead of substitution [15].

Thermal treatment has been applied with varying degrees of success to many different zeolites, aluminophosphates, silico-aluminophosphates (SAPOs), and mesoporous silicas. In general, extents of reaction (i.e., degree of nitridation) are highly dependent on the reaction conditions used. For example, treatment at 850°C may result in an increase in catalytic activity, whereas treatment at 800°C may not [13]. Nitrogen substituted zeolites, SAPONs, and AlPONs have been reported to have moderate to high activity in several base-catalyzed reactions, including the Knoevenagel condensation of benzaldehyde with malononitrile [11,13,14,16–19], ethyl cyanoacetate [11,19,20], propanedinitrile [21], or diethyl malonate [11]; and ethylation of ethylbenzene with ethanol [22]. The mechanism of the Knoevenagel reaction for the benzaldehyde/malononitrile case is shown in scheme 1. The selectivity is typically enhanced relative to non-zeolitic catalysts [22], sometimes completely inhibiting a competing reaction pathway [16,20]. The catalytic activity of substituted zeolites has been reported to increase with Si/Al ratio [21], and also increases (slightly) with nitrogen exposure time [18]. However, it has also been reported that higher nitridation temperatures cause a *decrease* in the catalytic activity [14]; as such, further work is needed to investigate this trend.

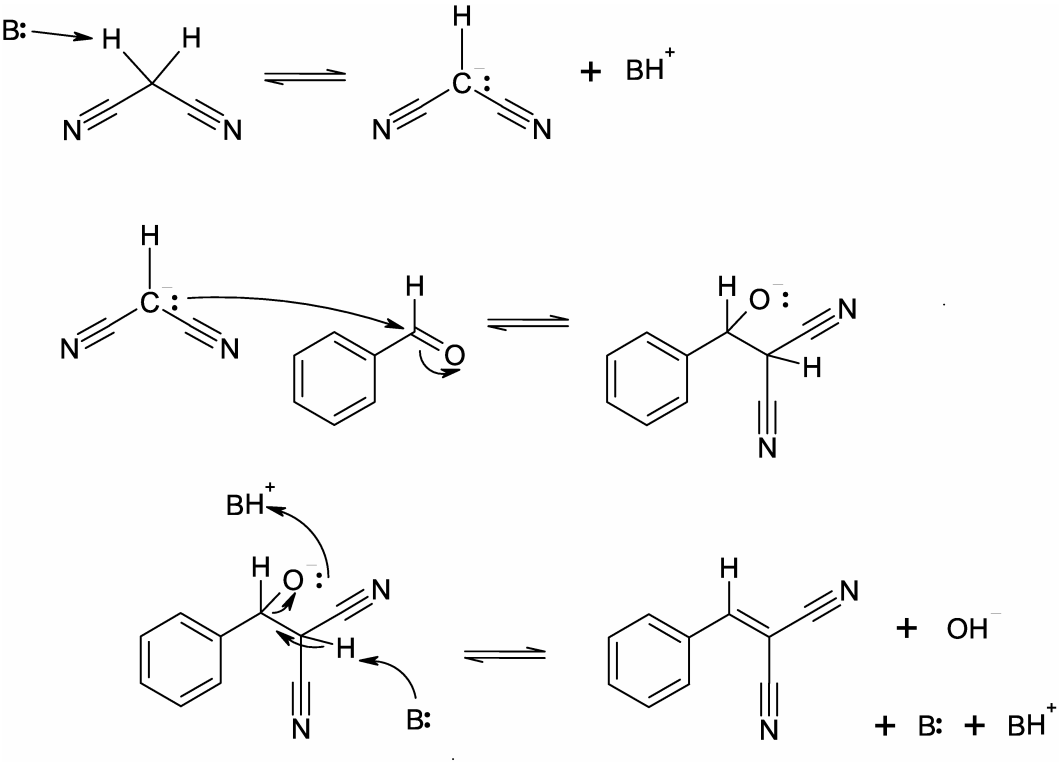

Scheme 1. Mechanism of the Knoevenagel condensation of malononitrile with benzaldehyde.

Nitrogen-substituted zeolites have been characterized by NMR spectroscopy [17,20,23–28] and infrared spectroscopy [3,11,16,18,21–23,29–33] to establish or rule out the presence of nitrogen in the structure. In general, infrared does not appear to be diagnostic of nitrogen substitution, and in some cases peaks in the IR spectrum appear in allegedly substituted materials that are not seen in materials synthesized by others [29,33]. On the other hand, NMR spectra seem to provide more direct evidence of nitrogen substitution. For AlPONs, ^{31}P NMR shows two or more peaks at high frequencies (near +25 ppm) [20,23,32]. Aluminum-27 NMR shows a set of new peaks at 13 ppm [20,23,32] and possibly −12 ppm [23] for SAPONs and ALPONs; 66 and 72 ppm [24] for zeolites. The ^{29}Si NMR spectra of nitrogen substituted zeolites and amorphous silicas [17,25–27] show an unmistakable peak near −90 ppm that corresponds to nitrogen substitution; similar peaks are seen in the spectra of oxynitride glasses [34–36]. A recent modeling study has been reported by us that confirms the ^{29}Si peak assignments [37] (see section 4), but further work is needed to confirm the ^{31}P and ^{27}Al assignments.

The extreme conditions of temperature used during thermal treatment are very likely to result in damage to the zeolite structure. It is also unclear where, precisely, nitrogen is likely to substitute under such conditions, and whether extents of reaction calculated from elemental analysis or alkaline digestion techniques are a good representation of the actual nitrogen content of the framework. Our knowledge of the precise NMR and IR spectral fingerprints of nitrogen substituted zeolitic materials remain incomplete. These issues provide a welcome entrance for simulation-based techniques.

3. CALCULATION OF SPECTROSCOPIC PROPERTIES

3.1. PERIODIC VS. CLUSTER CALCULATIONS

Many concerns relevant to zeolite modeling and theory in general are summarized by van Santen [38]; this section discusses issues specific to spectroscopic models and models directly relevant to amine and alkyl substitutions in zeolitic materials. The first question one must answer in any calculation involving solids is which of two approximations to make: the cluster approximation, in which small pieces of the solid (terminated by hydrogen) are simulated; or the periodic approximation, in which one or possibly more cells are simulated and the rest of the zeolite is assumed to exactly replicate the cell(s) being simulated in periodic fashion. Each formalism has its advantages and disadvantages.

In a periodic calculation, a group of one or more unit cells is simulated and the boundaries of the cell are modeled as being connected to another cell identical to the first. One advantage of this approach is that there is no need for artificially enforced constraints (other than symmetry), meaning the zeolite structure is relatively free to distort in the presence of defects such as nitrogen substitutions. The downside of this is that placing one nitrogen substitution in the framework has the effect of producing an infinite number of nitrogen substitutions, equally spaced in the real material, each one unit cell apart in all directions.

Cluster calculations involve clipping out parts of the zeolite into small pieces that can be simulated using localized basis sets. The edges of the cluster are terminated with hydrogen to avoid “dangling” bonds at the edges. This effectively treats that portion of the zeolite as a molecule, the premise being that local portions of the zeolite will have the

same properties as the quasi-infinite solid. This is a reasonable assumption because zeolites are electronic insulators, meaning their valence electrons exist in relatively localized states that are virtually unperturbed by cluster termination. However, it also makes the assumption that the local minimum-energy geometry—the collection of bond angles and bond lengths—is the same as it would be in the solid. For zeolites in particular, this assumption breaks down at the cluster's hydrogen-terminated edges: the difference in the chemistry between hydrogen and the rest of the atoms in the cluster is enough to cause the zeolitic structure to distort or even collapse, leaving one with—at best—a model of amorphous silica. To prevent this, the terminal atoms of the cluster are typically fixed at crystallographic positions during geometry optimization. It should also be mentioned that in silicates, there are two possible ways to terminate clusters: ≡Si–H bonds and ≡SiO–H bonds. Using Si–H bonds suffers from the fact that hydrogen and oxygen are *very* different chemically. Termination with silanol (≡SiO–H) groups can impair convergence of geometry optimizations through unstable Si–O–H bond angles; this problem can be avoided by freezing both the oxygen and hydrogen atoms of the OH groups. In some cases, the extra "layer" produced by ≡SiO–H termination (in contrast to ≡Si–H termination) yields better convergence with respect to cluster size [39].

Some of the limitations of the cluster approximation can be alleviated by using *hybrid* clusters, also known as *embedded clusters*. In an embedded cluster, electronic energies are calculated using two or more computational approaches: a relatively accurate approach in the heart of the cluster where chemical and/or spectroscopic information is sought, and subsequently less accurate (and computationally less expensive) approach(es) farther away. The most common approach—dubbed QM/MM (Quantum Mechanics/Molecular Mechanics)—is to use an all-electron quantum description in the heart of the cluster, and a force field for the rest of the system. For zeolites, this approach allows the approximate treatment of an entire zeolite cage and its steric constraints, without having to represent all the associated electrons. In the case of a two-layer embedding with "high" and "low" levels of theory, the energy of the entire system is estimated according to:

$$E_{\text{large,low}} + (E_{\text{small,high}} - E_{\text{small,low}}), \tag{1}$$

where the first term is the low-level description of the large system (both layers), and the second term in parentheses is the high-level correction that avoids double-counting the small system (inside layer).

Various embedding approaches differ in their definitions of "small" and "large" systems, and how "inside" and "outside" layers are coupled. These issues are of particular importance for modeling network solids such as silica, which require cutting of bonds when defining layers. As a result, essentially all embedding approaches applied to silica terminate dangling bonds in the inside layer by adding capping atoms such as hydrogen (i.e., "small system" = "inside layer" plus capping hydrogens). Regarding the "large system," the QM–Pot approach of Sierka and Sauer represents this with an accurate force field and periodic boundary conditions at fixed volume [40,41]. In contrast, the ONIOM [40] calculations of Fermann *et al*. [39] applied a generic force field and treated the large system as a very large, isolated cluster with fixed terminal atoms. (ONIOM, developed by Morokuma and coworkers, stands for "the authors' Own *N*-layered Integrated molecular Orbital molecular Mechanics scheme" [40].) Both methods were applied to modeling acid sites in zeolites, and obtained essentially identical results. One final issue regards modeling the back-and-forth polarization of inside and outside layers, also known as "electronic embedding." This is very difficult to get right. For example, allowing the outside layer to polarize the inside electron density, *but not vice versa*, can lead to over-polarization, which can reduce accuracy. Because of this, the calculations of Sierka and Sauer, and those of Fermann *et al*., do not include electronic embedding, and as such are referred to as "mechanical embedding."

Clusters are the only practical choice for all-electron calculations on zeolite frameworks with large cells such as FAU (e.g., HY) and MFI (e.g., ZSM-5), as full periodic calculations take on the order of months for such systems. This is not a reflection of the speed of modern computers, but one of scaling. For example, the processor time required to perform Hartree–Fock calculations and many Kohn–Sham density functional theory (DFT) calculations scale with the number of (non-primitive) basis functions to the third power [42]. Assuming this scaling, a calculation that takes two hours for the SOD framework (36 atoms, 360 electrons) would take on the order of 300 *days* for the FAU framework (576 atoms, 5760 electrons). As such, it is often

advisable to use cluster calculations for effects, such as NMR, that can be realistically modeled with clusters. In other cases, it may be possible to do a calculation on silica MFI (288 atoms) using simplified descriptions of the core electrons [43], and/or using a different description of the unit cell. The latter is particularly useful for the FAU structure, which has a 576-atom cubic unit cell but can also be described by a 144-atom rhombohedral cell [44,45].

The periodic approximation is better suited in many cases to study vibrational spectra. A vibration that involves the atoms in a ring, for example, would likely be poorly simulated by a cluster model since one or more of those atoms would be near another atom that has been fixed at its crystallographic coordinates. However, if one is careful about including *only* vibrations that result from atoms relatively far from the edges, clusters can yield excellent results from vibrational calculations, especially when layered methods are employed [46]. Care must *always* be taken to remove vibrations from atoms whose coordinates are fixed during geometry optimization: these nuclei are *not* at local minima on the adiabatic surface (which is explicitly assumed in most vibrational calculations), and the calculation of their vibrations will therefore result in spurious imaginary frequencies.

3.2. THEORETICAL CONSIDERATIONS

Predictive calculation of accurate spectroscopic information in zeolites often requires a quantum mechanical treatment, though modern force field parameterizations show much promise for the calculation of vibrational spectra [47–49]. Common methods employed are Hartree–Fock theory, Kohn–Sham density functional theory (DFT) [50], and Møller–Plesset perturbation theory [51]. Methods that include substantial amounts of correlation energy, such as coupled cluster theory (CC) and configuration interaction (CI), are nearly useless for zeolites, as the calculations scale poorly with system size—CC scales with N^6 to N^8, where N is the number of basis functions, and CI scales as $N^{6–10}$ or even $N!$, depending on the number of interactions used [42]. Even MP2 (second-order perturbation theory) typically requires forbidding amounts of memory and processor time (the latter scaling as N^5 [42]) to be useful for zeolites. For comparison, a calculation of the energy of a dimerized pair of benzene molecules (84 electrons) takes about 35 *seconds* at B3LYP/6-311G(*d*,*p*); the same calculation at MP2/6-311G(*d*,*p*) takes about

150 s (over four times longer) and over an hour (over 100 times longer) at CCSD. This means that a calculation that takes six hours using DFT would take *fifteen months* with CCSD!

The calculation of molecular properties, including infrared and Raman frequencies and intensities and NMR shielding constants, is covered in an excellent review by Gauss [52]. Methodologies for each of these are touched on in the rest of this section.

3.2.1. Calculation of Nuclear Shielding (NMR)

Here we present a brief review of the methodological aspects of modeling NMR spectra. What follows is generically applicable to modeling NMR spectra of any chemical species, including ^{29}Si NMR, which is the central method of characterizing silica-based materials. Calculating shielding tensors (σ) for nuclei in the presence of a magnetic field (**B**) requires the introduction of a vector potential (**A**). Any number of vector potentials **A** can be defined that produce the same magnetic field. Going from one such vector potential to another is called a *gauge transformation*. The usual choice of gauge is *Coulomb gauge*, where **A** is chosen so that $\mathrm{div}\,\mathbf{A} = 0$. A uniform magnetic field of known strength is always assumed in calculations, since every effort is taken in real NMR spectrometers to place the sample close enough to the center of the solenoidal field that the magnetic field can be approximated as uniform there. The (somewhat circular) definition that is typically used is $\mathbf{A} = \mathbf{B} \times (\mathbf{r} - \mathbf{R_G})$, where **r** is the position vector and $\mathbf{R_G}$ is an arbitrary vector called the *gauge origin*. Using one gauge origin to define the vector potential badly miscalculates magnetic properties due to the incomplete description of the wavefunction (see, for example, Fig. 1 of Ref. 53), so the use of so-called *distributed gauge origin* methods has become prevalent.

For cluster calculations, the most common distributed gauge theories are the Individual Gauge for Localized Orbitals (IGLO) [54], the Continuous Set of Gauge Transformations (CSGT) [53] and the closely-related Individual Gauges for Atoms in Molecules (IGAIM) [55], and Gauge-Including Atomic Orbitals (GIAO) [56,57]. The details of these methods are discussed in some detail by Gauss [52]; each is a different formalism for removing the spurious effects of gauge origin placement. Two methods have been developed by Mauri, Pfrommer, and Louie (MPL) [58] and Charpentier et al. (GIPAW) [59] that implement NMR calculations for periodic systems.

There exist several convergence studies that determine which method (GIAO, CSGT, etc., as well as HF, DFT, etc.) is "the best" for calculating nuclear shielding constants. Unfortunately, we are unaware of a study that has focused on silica-based materials, to date. Cheeseman and coworkers [60] tested GIAO vs. CSGT using Hartree–Fock and DFT calculations with several density functionals and found that, with the notable exception of the local spin density approximation (LSDA), density functional theory using both "pure" and "hybrid" exchange–correlation functionals gives a smaller root-mean-square error with respect to experimentally determined chemical shifts than does Hartree–Fock. They also concluded that GIAO:B3LYP/6-311+G(2*d*,*p*) predicts quantitatively accurate ^{13}C chemical shifts and reasonable ^{15}N and ^{17}O chemical shifts, but at a fraction of the computational resources required for the corresponding MP2 calculation. Another study by Magyarfalvi and Pulay [61] indicated that OPTX (or "OPTimized eXchange") exchange functional [62] with the Lee–Yang–Parr correlation functional [63] (OLYP) outperforms the BLYP functional [64,65] for ^{13}C, ^{15}N, and ^{17}O nuclei. Sefzik and coworkers [66] found that DFT in general outperforms Hartree–Fock calculations, noting that hybrid functionals like B3LYP [63,64,67–69], B3PW91 [64,69–71], and mPW1PW91 [70–73] provide the best ^{13}C shielding tensors for single crystals. Another study [74] recommended the OPBE functional [62,75,76]. Moon and Case [77] found that HF and DFT differed systematically from MP2, and small basis set values were often fortuitously closer to experimental values for chemical shifts in peptides. Baldridge and Siegel [78] have even suggested using empirical scaling factors to obtain chemical shifts from computed shielding constants, in analogy with the vibrational scaling factors discussed below.

In general, GIAO shows the fastest convergence with respect to number of basis functions for most nuclei [60,79], though it has been reported that differences between GIAO and CSGT are negligible with the use of plane-wave basis sets for valence electrons [80], which are used in most periodic electronic structure programs such as VASP. While true accuracy in chemical shielding can only be obtained by very accurate, expensive calculations such as CCSD(T) (coupled cluster theory with single and double excitations and perturbative triple excitations) to describe electron correlation [81], the results of DFT and MP2 calculations are generally found to be of intermediate accuracy

between HF and CC calculations. Due to the drastic differences in computational expense between HF and CC methods [42], DFT remains the best option. Several density functionals have been proposed that are parameterized with shielding tensors in mind [82-85], but until these functionals have been implemented and thoroughly tested, a recommended starting point for NMR calculations on clusters is GIAO with a relatively large basis set (at least triple-zeta basis sets, e.g., 6-311+G(2*d*,*p*) [86,87] or cc-pVTZ [18,88–93], are recommended to obtain reasonably converged chemical shifts) and a density functional such as B3LYP or OLYP.

3.2.2. Calculation of Vibrational Spectra

There are far fewer issues in calculating vibrational quantities from electronic structure calculations than with magnetic properties. This is due to the fact there is no gauge origin or similar concept to obscure the calculation. The basis behind vibrational calculations is the series

$$V(x) = V(0) + \left.\frac{dV}{dx}\right|_{x=0} x + \frac{1}{2}\left.\frac{d^2V}{dx^2}\right|_{x=0} x^2 + \cdots, \qquad (2)$$

where x is the spatial coordinate in the direction of one of the *normal modes* of vibration. The first term, $V(0)$, is simply the zero of energy and is arbitrary. The second term is zero at an energetic minimum on the adiabatic surface, so it too can be disregarded (assuming the geometry has been optimized and no atoms have been fixed!). For small deviations, the only important term that remains is the second-order term; this is the *harmonic oscillator* approximation. The (angular) vibrational frequency ω is determined from the second derivative according to $V''(0) = \frac{1}{2} m\omega^2$, where m is the reduced mass of the atoms involved in the vibration. The vibrational *wavenumber* in units such as cm^{-1} is given by $\omega/2\pi c$, where c is the speed of light.

Most programs calculate vibrational frequencies for multi-dimensional systems by constructing a matrix of second derivatives and differentiating the potential energy with respect to mass-weighted atomic Cartesian coordinates [94]. The resulting matrix is called the Hessian or the force-constant matrix. Because of the mass weighting, the matrix elements have units of frequency squared. This matrix is then diagonalized, yielding normal-mode frequencies (square roots of eigenvalues) and normal-mode vibrational coordinates (eigenvectors). For large systems, the matrix construction and

diagonalization can quickly become intractable. When computing vibrational frequencies for localized vibrations (e.g., for rate coefficient computations), layered calculations can be used to increase system size without adding as much complexity to the calculation [95].

Most electronic structure methods tend to overestimate vibrational frequencies because of insufficient treatment of "correlation energy" (difference between exact and Hartree–Fock energies) [96]. For example, the Hartree–Fock method over-emphasizes ionic configurations, causing overestimates of both dissociation energies and vibrational frequencies. As such, it has been proposed that calculated frequencies be scaled to obtain agreement with experimental spectra ([96,97] and citations therein). The scaling factors are typically 0.89–0.91 for Hartree–Fock calculations, 0.96–1.01 for DFT with various functionals, and 0.93–0.96 for MP2. These scaling factors typically improve relatively high vibrational frequencies, though low frequency vibrations are not improved to the same extent. Scaling the vibrational frequencies also has an effect on the zero-point energy, internal (thermal) energy, enthalpy, entropy, and free energy calculated from these frequencies as well. In the case of zero-point energy, scale factors have been published, though another option is to use scaled frequencies in the calculation of the zero-point energy.

3.3. CALCULATION OF INTENSITIES

The intensities of vibrational spectra—absorbance in infrared spectroscopy controlled by dipole moments, and scattering intensity in Raman spectroscopy controlled by polarizabilities—can be computed numerically or analytically. Analytic second-derivatives, required for infrared intensities [98], have been implemented for a large fraction of electronic structure methods [52, p. 16], and should be used when available. Analytic *third* derivatives, required for Raman intensities [99], are much less common [52, p. 16]. As such, Raman intensities are often calculated numerically. Computing Raman intensities—analytically *or* numerically—requires excessive resources in addition to those required for a vibrational calculation.

Intensities in NMR spectra—so-called *integrals*—are a function not of the intensity of absorption but the number of nuclei with the same chemical environment in the entire material. In a periodic calculation, this is simple: add one intensity unit to the chemical

shift for each nucleus in the crystal and sum over all nuclei. In cluster models, this summation *must* be restricted to nuclei that are far enough (three layers [100]) from the boundary to represent actual electron densities.

A possible shortcut to simulating the entire crystal hundreds of times exists, however: if the distribution of chemical environments can be estimated somehow, one merely needs to simulate each chemical environment *once* and then multiply by that intensity. In siliceous zeolites, the number of distinct silicon chemical environments is (to very good approximation) the number of symmetrically inequivalent tetrahedral (T) sites in the crystal. These considerations were used by Sauer and coworkers to simulate the ^{29}Si NMR spectra of siliceous MFI, MEI, MTW, TON, FAU, and α-quartz [100] as well as FER [101]. This approach was also used by us to simulate ^{29}Si NMR spectra of nitrided zeolite HY (see section 4) [37].

If aluminum or another heteroatom is present, this produces a distribution of five peaks (corresponding to silicon near 0, 1, 2, 3, and 4 heteroatoms) that is imposed on each T-site's chemical shift. Due to Loewenstein's rule [102], which precludes Al–O–Al linkages in zeolites because of electrostatic repulsion, all aluminum atoms in the cell can be counted by summing over silicon atoms. This fact was observed by Melchior and coworkers [103,104] and exploited by Vega [105] to predict integrals for the FAU structure. This is possible because the FAU structure has only one symmetrically distinct T-site. In crystals that possess less symmetry, the number of required calculations goes up dramatically. For example, the low-temperature form of ZSM-5 (MFI framework) contains 24 distinct tetrahedral sites, multiplied by five possible aluminum environments per silicon, or 120 calculations to produce the NMR spectrum. The use of higher symmetry environments is therefore very expedient.

3.4. SYSTEM SIZE EFFECTS

Both cluster and periodic calculations require consideration of system size effects. This is obvious for silica clusters because cluster termination can corrupt nearby electron distributions. System size also influences periodic calculations through unit-cell size; this controls the allowed densities of defect structures and adsorbed guest molecules. For vibrational spectra, low-frequency framework vibrations (usually Raman-active) will likely be blue-shifted by cluster termination and the associated constraints. System-size

convergence studies are therefore required. Nuclear shielding, on the other hand, can be a much more local phenomenon when studying localized electronic states such as those in silicates.

For zeolites and similar materials, Bussemer and coworkers [100] showed that a cluster with three "layers" of atoms is sufficient to converge chemical shifts with respect to system size. As such, all that is required is to build a cluster wherein all terminal hydrogen atoms are at least three bonds away from the atom one is interested in. Unfortunately, clusters get large—and the calculations become intractable—rather quickly. The number of atoms goes up, naïvely, with L^3, where L is the number of layers. In addition, one must be careful that the bonds that are "cut" to form the cluster are not bonds from two different tetrahedral atoms to the same oxygen atom—such a cut would force two cluster-capping protons to be in close proximity, drastically distorting the electron density and straining the other chemical bonds in the cluster. In zeolite-like materials, this can be avoided by obeying a simple rule: never leave out only one tetrahedral atom in a ring.

Taking the FAU structure as an example, there are certain cluster sizes that constitute the minimum one can use corresponding to a certain number of layers of atoms away from a central tetrahedral atom. If 2T denotes a structure with two tetrahedral atoms (typically T = Si, Al, or P, but could also be Ge, Ga, B, or a number of other atoms), then the increments in clusters are from 1T to 8T to 23T, which represent 1, 3, and 5 layers of atoms from the central tetrahedral atom, respectively (see Figure 2). Note that layers of two and four atoms are not possible due to the need to complete four-membered rings. The number of total atoms jumps from 9 to 42 to 102, and the number of electrons jumps from 50 to 300 to 800. Such large computations are often intractable (see the comments on scaling in section 3.2), so starting from an 8T cluster (or possibly the 8T cluster in Figure 2 mirrored on itself to produce a 10T or 12T cluster with *two* tetrahedral atoms far enough from the edges) is recommended.

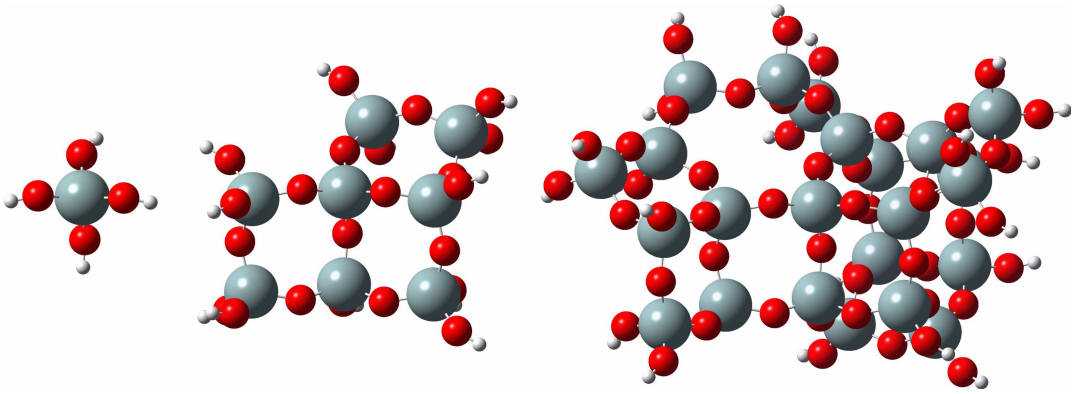

Figure 2. Examples of clusters cut from the FAU framework. White: hydrogen; light gray: silicon; dark gray: oxygen. *Left:* 1T cluster (one layer around central T atom, 9 atoms, 50 electrons). *Middle:* 8T cluster (three layers, 42 atoms, 300 electrons). *Right:* 23T cluster (five layers, 102 atoms, 800 electrons).

3.5. CHOICE OF NMR REFERENCE

Calculations of magnetic shieldings return only the *shielding tensor*. Reporting chemical shifts therefore requires the use of a reference nucleus, analogous to the reference used in experiments. The standard experimental references for most nuclei are liquids, and since electronic structure calculations are inherently gas-phase calculations, a secondary reference is usually more convenient and/or accurate. The chemical shift can then be computed as

$$\delta = \frac{\sigma_{\text{ref}} - \sigma}{1 - \sigma_{\text{ref}}} + \delta_{\text{ref}} \approx \sigma_{\text{ref}} - \sigma + \delta_{\text{ref}}, \tag{3}$$

where σ is the shielding constant (defined as a third of the trace of the shielding tensor), σ_{ref} is the shielding constant of the secondary reference molecule, and δ_{ref} is the chemical shift of the secondary reference relative to the primary reference, preferably in the limit of zero pressure.

Common secondary references for silicon NMR are gaseous TMS ($\delta = 0$ ppm) [106,107], solid quartz ($\delta = -107.4$ ppm) [101,108], and silane (SiH_4) in the limit of zero pressure ($\delta = -104.34$ ppm) [109]. For oxygen NMR, gaseous water can be used ($\delta = -36.11$ ppm from liquid water) [110]. For hydrogen NMR, TMS ($\delta = 0$ ppm), methanol ($\delta = 0.0197$ ppm) [111,112], or silane ($\delta = 5.150$ ppm) [109] can be used. The best references of which the authors are aware for nitrogen NMR is ammonia ($\delta = -400.29$ ppm from liquid nitromethane) [113]. References in the gas phase for ^{27}Al NMR are difficult to find due to the tendency of aluminum to form solids. Valerio and Goursot [106] recommended dimerized trimethylaluminum (TMA) as a secondary

reference, but $Al(H_2O)_6^{3+}$ with water molecules arranged in an octahedral coordination (δ = 0 ppm) remains the safest choice.

4. MODELING NITROGEN-SUBSTITUTED ZEOLITIC MATERIALS

As mentioned in the Introduction, the base strengths of zeolite frameworks are typically weak. Barthomeuf [114] found that a rough ordering of the "intrinsic basicity" of the framework oxygens for various zeolite frameworks is FER > MFI > MOR > MWW > BEA > LTL > FAU. However, much work has been done to increase the base strength and modify other material properties by substituting oxygen atoms with amine or methylene groups in the zeolite framework, as discussed in section 2. A significant amount of work has been done recently to model the properties and assist in the characterization of these intriguing materials.

Early work by Corma and coworkers [115] predicted the energetics and vibrational spectra of the nitrogen substitution reaction in both silicates and aluminophosphates. Their calculations, based on the small molecules $H_3SiOSiH_3$ and H_3AlOPH_3, studied reactions with ammonia to form water and both substitution and bond-cleaving sites. The energies of reaction with ammonia to form water and the resulting amine are shown in Table 1. They concluded that substitution at terminal sites (≡Si–NH_2 and ≡P–NH_2) is a favorable reaction, since the calculations showed an *exoergic* (the analog of exothermic for potential energy) reaction. However, a subsequent study by the authors [37] showed that substitutions at terminal sites in zeolites, which are more properly modeled as substitution of Si–OH for Si–NH_2 rather than Si–H for Si–NH_2, are still endoergic to the tune of approximately +30 kJ/mol. We did confirm, however, that substitution at terminal sites is *less* energetically unfavorable than substitution at framework sites.

Table 1. Energies of reaction for [Reactant] + NH_3 → [Product 1] + [Product 2]

Reactant	Product 1	Product 2	ΔE (kJ/mol)
$H_3SiOSiH_3$	$H_3SiNHSiH_3$	H_2O	118
$H_3SiOSiH_3$	$H_3SiOSiH_2NH_2$	H_2	−28.9
$H_3SiOSiH_3$	H_3SiOH	H_3SiNH_2	76.2
H_3AlOPH_3	$H_3AlNHPH_3$	H_2O	113
H_3AlOPH_3	$H_3AlOPH_2NH_2$	H_2	−23.9
H_3AlOPH_3	H_3AlNH_2	H_3POH	632
H_3AlOPH_3	H_3AlOH	H_3PNH_2	533

The same study by Corma and coworkers [115] predicted a change in vibrational frequency of 50–100 cm^{-1} for the NH stretching modes between bridging and terminal NH substitutions. Similar studies by Fleischer and coworkers computed vibrations for disilylamine ($H_3SiNHSiH_3$) [116] and methyldisilylamine ($H_3SiNCH_3SiH_3$) [117] as well, scaled by factors similar to those discussed in section 3.2.2. The calculations allowed them to assign the bands at 827 and 745 cm^{-1} to in-plane and out-of-plane silyl rocking motions. It also confirmed the assignments of the Si–N–Si symmetric stretch at 610 cm^{-1} and the δSiNSi band at 200 cm^{-1} for disilylamine.

Márquez and coworkers [118] studied the phosphorus and aluminum NMR spectra of nitrogen substituted aluminum phosphate (AlPON) clusters using a 4T model. Their clusters were designed to model substitutions near portions of (amorphous) AlPO where aluminum and phosphorous do *not* alternate, in an attempt to determine the preferred site for substitution. This assumes the AlPO in question is a "solid solution" of $AlPO_4$, Al_2O_3, and Na_3PO_4. They computed ^{31}P and ^{27}Al shielding constants for their clusters using GIAO:HF/6-311G(2*d*,*p*) to confirm spectral assignments observed experimentally. The observed difference from PO_4 tetrahedra to PO_3N tetrahedra ($\Delta\delta_P$ = 20.8 ppm) agrees well with experiment ($\Delta\delta_P$ = 23 ppm), but the observed difference from AlO_4 tetrahedra to AlO_3N tetrahedra ($\Delta\delta_{Al}$ = 18 ppm) was not observed experimentally—instead, very little difference was observed in the ^{27}Al spectrum. They concluded that substitution occurs preferentially at any ≡P–O–P≡ bridges that exist in the structure, followed by ≡Al–O–P≡ bridges, and then any Al–O–Al bridges that exist (by arguments similar to Loewenstein's rule [102], all Al–O–Al bridges would necessarily be bonded to at least one octahedrally coordinated aluminum species).

The experimental synthesis of zeolitic structures with Si–CH_2–Si connectivity by Yamamoto and coworkers [119] inspired Astala and Auerbach [120] to test the stability of zeolite frameworks by computing the additional strain energy. Using periodic calculations on the SOD and LTA frameworks, they compared the zeolite energies to appropriate (unstressed) polymeric reference molecules and found that the strain caused by an amine or methylene substitution was partially offset by changes in the bond angles and lengths of surrounding Si–O–Si bonds. The result is a substituted framework with

relatively little strain (~0.1 eV per defect) relative to the unstressed, unsubstituted zeolite. Results of calculations with constant and variable lattice parameters (i.e., length of one side of the cubic unit cell) indicated that the unit cell expands or contracts to offset strain. Perhaps their most important result was to confirm intuition about base strength: Si–OH–Al was found to be a stronger acid than Si–NH_2–Al, while the base strength of Si–NH–Si is roughly twice that of Si–O–Si, determined by calculating BF_3 adsorption energies.

Waroquier and coworkers [121] took the idea of increased base strength one step further and performed simulations on zeolite clusters that contain both an amine substitution (Si–NH–Si or Si–NH–Al) and a Brønsted–Lowry acid site (Si–OH–Al) in close proximity. Their goal was to predict changes in the reaction pathway for alkoxide and/or alkylammonium formation in zeolites as the first step in methanol to hydrocarbon conversions. Such reactions are thought to require a relatively strong acid and at least a weak base to proceed; alkoxides are the intermediates in acid zeolites, and alkylammonia would occur in zeolites with amine substitutions. Calculations on 4T clusters and 5T ring-shaped clusters using DFT with B3LYP/6-31G(*d*) predicted that the activation energy for an acid site (O–Al–OH) is 161 kJ/mol, while the activation energy for a similar site with both an acid *and* an amine site (NH–Al–OH) is only 133 kJ/mol. They observed a similar trend (170 vs. 118 kJ/mol) with the ring-like structure. Unfortunately, they were forced to conclude that such a structure would be impossible to synthesize in reality: the hydrogen atom from the (strongly acidic) OH site would, in a real material, jump to the other side of the aluminum atom to neutralize the (strongly basic) amine site, producing a weak-acid/weak-base product of the form NH_2–Al–O. As a result, they modeled a bifunctional acid/base cluster wherein the base site was on one side of the ring and the acid site on the other [122]. While this particular structure might still be difficult to target synthetically, it would at least remain stable once formed. For methoxide/methylammonium formation from chloromethane, their 16T clusters showed a reduction in activation energy from 196 kJ/mol over an acidic cluster to 163 kJ/mol over a dual acid-base cluster with the NH group on the opposite side of the 5T ring. Waroquier and coworkers commented that this barrier reduction is expected to be most pronounced for highly strained transition states.

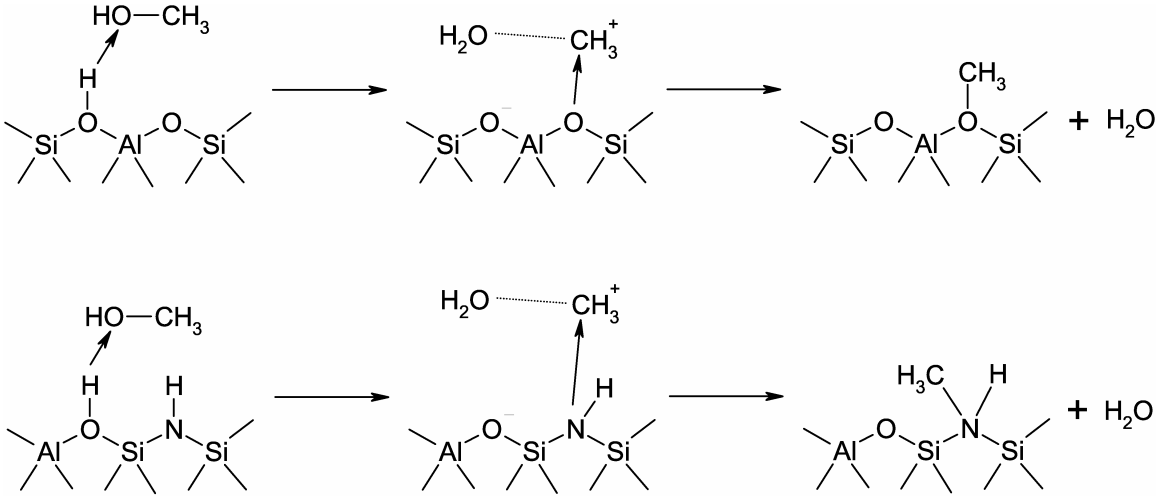

Scheme 2. Reaction mechanism for the formation of alkoxide (top) and alkylammonium (bottom) species in a zeolite with (top) and without (bottom) nitrogen substitutions. Adapted from Ref. [122].

Zheng and coworkers [123] sought to determine the barrier to neutralization that an adjacent pair of acid and base sites (e.g., Si–NH–Al–OH–Si) would encounter. The difference in energy between Si–NH–Al–OH and Si–NH_2–Al–O was found to be +32.7 kJ/mol based on a layered (ONIOM [124]) calculation, with activation energies of 49.4 and 16.7 kJ/mol for forward and backward conversion between the two. They went on to conclude that the first step in ethylene protonation over ammonia-treated zeolites is proton transfer from the NH_2 group to form an OH and NH group (i.e., Si–OH–Al–NH–Si). It is this group that then reacts with the ethylene molecule, which forms an ethylammonium complex. The barrier for the rate-limiting step in ethylene protonation was calculated to be 49.4 kJ/mol for the amine-substituted ZSM-5 catalyst, compared to 90.2 kJ/mol in unsubstituted ZSM-5. The energy of adsorbed ethylammonium ion is also significantly lower than the energy of ethoxide ion, meaning ethylene protonation is both thermodynamically and kinetically more favorable over N-ZSM-5 than ZSM-5.

Finally, we address recent work on the *location* of substitutions in zeolite frameworks. Wu et al. [125] studied the MFI structure to determine which of the 26 symmetrically distinct oxygen sites in the orthorhombic framework were most likely to react during nitridation. They found that the substitution energy at each site increases in the order $O^{21} < O^{11} < O^4 \approx O^{26} < O^5 < O^{15} << O^1 \approx O^{10} \approx O^{25} < O^8 < O^{24} \approx O^{17} < O^{18} \approx O^{20} < O^{23} \approx O^{14} < O^9 < O^6 < O^{16} \approx O^2 < O^7 < O^{19} < O^{12} < O^3 < O^{13}$ using the standard numbering system [126]. They concluded that this will most likely result in a nitrogen substitution near an acid site, since the T^{12} site (to which O^{11} is bound) is a likely site of aluminum

substitution [127]. Nitrogen substitution would therefore be more likely to decrease the strength of the acid site (i.e., substitute Si–OH–Al for Si–NH_2–Al) rather than creating a new basic site (Si–NH–Si).

We recently addressed the issue of the location and energies of nitrogen substitution in the FAU framework [37], using NMR spectroscopy as a semi-quantitative measure of the extent of reaction (i.e., what fraction of oxygen atoms have been replaced by nitrogen). Our calculations employed a 14T cluster containing two atoms at least three "layers" away from the terminating hydrogen atoms. Chemical shifts were calculated with GIAO:B3LYP/cc-pVTZ, with silane as a secondary reference. Since the FAU structure has only one crystallographically distinct silicon atom, we simulated the NMR spectrum by assuming Vega's distribution of aluminum [105] and a random distribution of nitrogen among the acid sites. We hypothesized that the acid sites should fill first: the substitution energy for the reaction zeolite + NH_3 → N-zeolite + H_2O was about 30–35 kJ/mol for substitution at an acid site and 98–110 kJ/mol for substitution between two silicon atoms. To fit the experimental spectrum, we employed a Lorentzian line shape of a fixed width (a fitting parameter) and adjusted the substitution ratio (N/(N + O)) to obtain an estimate of the extent of reaction. This technique holds promise for the simulation of the NMR spectra other frameworks, though the FAU zeolite was chosen because of its high symmetry. The results show that high levels of nitrogen substitution can be achieved while maintaining porosity, particularly for NaY and low-aluminum HY materials, without significant loss in crystallinity. Comparison of simulated NMR spectra with experiments performed at lower temperatures (750–800 °C) show a preference for substitution at Si–OH–Al sites. No preference is seen for reactions performed at higher temperatures and longer reaction times (e.g., 850 °C and 48 hours).

5. SUMMARY

The use of electronic structure calculations to model nitrogen substitutions in zeolites and related materials has provided some very important insights into the synthesis and characterization of these materials. The enormous task of modeling catalytic reactions that could potentially take place on these materials is largely in front of us. Initial calculations (section 4) have demonstrated that barriers to reaction can be reduced using substituted zeolites, though this is not guaranteed for every reaction (even those known to

work with different choices of base catalyst). The realm of spectroscopic modeling of zeolites has also come into its own in recent times. With NMR calculations, in particular, what was largely a tool for qualitative predictions only has now become a near-quantitative—if still developing—predictive method for some choices of material and computational method.

There are several important but as yet unaddressed problems related to the modeling of basic zeolites. The first is the prediction of the spectroscopic "signature" of substituted AlPONs and SAPOs, particularly in the ^{27}Al NMR where the effects of quadrupolar broadening are difficult to isolate experimentally. The question remains unanswered as to the nature of active site in base catalysis, though some promising hypotheses have been discussed (see section 4). Perhaps the most important modeling problem is the daunting number of substitution structures (> 100) that need to be considered for nitrided alumino-silicates.

The biggest question yet to be answered with regard to basic zeolites is this: Are these materials stable? Theoretical work can help with this issue by predicting the reaction pathways for substitution, a project currently under investigation by the authors. Further work—both experimental and theoretical—may help to determine the range of useful conditions and appropriate choices of reagents that can safely be used with zeolite catalysts.

ACKNOWLEDGMENTS

The authors are greatly indebted to Dr. Geoffrey Tompsett for his help in locating some relatively obscure experimental literature, much of which cannot be cited in this chapter for practical reasons. We also thank Prof. Justin Fermann, Prof. Curt Conner, and Vishal Agarwal at UMass Amherst, and Prof. Clare Grey and Fulya Dogan at SUNY Stony Brook, for helpful collaboration and discussion. Our research in this area is generously funded by the National Science Foundation (CBET-0553577) and the United States Department of Energy (DE-FG02-07ER15918).

REFERENCES

1. Auerbach, S.M., Carrado, K.A. and Dutta, P.K. (Eds.) 2003, Book Handbook of Zeolite Science and Technology, Marcel–Dekker, New York.
2. Hattori, H. 1995, Chem. Rev., 95, 537.

3. Kerr, G.T. and Shipman, G.F. 1968, J. Phys. Chem., 72, 3071.
4. Weitkamp, J., Hunger, M. and Rymsa, U. 2001, Micropor. Mesopor. Mater., 48, 255.
5. Barthomeuf, D. 1996, Catal. Rev. Sci. Eng., 38, 521.
6. Goodwin, J.G., Jr., Bruce, D.A., Lotero, E., Mo, X., Liu, Y., Lopez, D.E. and Suwanakarn, K. 2007, Heterogeneous Catalyst Development for Biodiesel Synthesis, Tech. Rep., U.S. Department of Agriculture.
7. Climent, M.J., Corma, A., Hamid, S.B.A., Iborra, S. and Mifsud, M. 2006, Green Chem., 8, 524.
8. Macquarrie, D.J. 1996, Chem. Commun., 1961.
9. Angeletti, E., Canepa, C., Martinetti, G. and Venturello, P. 1989, J. Chem. Soc. Perkin Trans. 1, 105.
10. Cauvel, A., Renard, G. and Brunel, D. 1997, J. Org. Chem., 62, 749.
11. Climent, M.J., Corma, A., Fornés, V., Frau, A., Guil-López, R., Iborra, S. and Primo, J. 1996, J. Catal., 163, 392.
12. Zhang, C.M., Liu, Q. and Xu, Z. 2005, J. Non-Cryst. Solids, 351, 1377.
13. Ernst, S., Hartmann, M., Sauerbeck, S. and Bongers, T. 2000, Appl. Catal. A Gen., 200, 117.
14. Narasimharao, K., Hartmann, M., Thiel, H.H. and Ernst, S. 2006, Micropor. Mesopor. Mater., 90, 377.
15. Kerr, G.T. 1969, J. Catal., 15, 200.
16. Delsarte, S., Aurou, A. and Grange, P. 2000, Phys. Chem. Chem. Phys., 2, 2821.
17. Zhang, C.M., Xu, Z., Wan, K.S. and Liu, Q. 2004, Appl. Catal. A Gen., 258, 55.
18. Srasra, M., Poncelet, G., Grange, P. and Delsarte, S. 2005, Stud. Surf. Sci. Catal., 158, 1811.
19. Massinon, A., Odrizola, J.A., Bastians, P., Conanec, R., Marchand, R., Laurent, Y. and Grange, P. 1996, Appl. Catal. A Gen., 137, 9.
20. Xiong, J.M., Ding, Y.J., Zhu, H.J., Yan, L., Liu, X.M. and Lin, L.W. 2003, J. Phys. Chem. B, 107, 1366.
21. Ernst, S., Hartmann, M., Hecht, T., Jaen, P.C. and Sauerbeck, S. 2002, Stud. Surf. Sci. Catal., 142, 549.
22. Guan, X., Li, N., Wu, G., Chen, J., Zhang, F. and Guan, N. 2006, J. Mol. Catal. A Chem., 248, 220.
23. Stein, A., Wehrle, B. and Jansen, M. 1993, Zeolites, 16, 249.
24. Yang, X. and Truitt, R.E. 1996, Zeolites, 16, 249.
25. Han, A.J., He, H.Y., Guo, J., Yu, H., Huang, Y.F. and Long, Y.C. 2005, Micropor. Mesopor. Mater., 79, 177.
26. Han, A.J., Guo, J., Yu, H., Zeng, Y., Huang, Y.F., He, H.Y. and Long, Y.C. 2006, ChemPhysChem, 7, 607.
27. Wakihara, T., Saito, Y., Tatami, J., Komeya, K., Meguro, T., Mackenzie, K.J.D., Takagi, S. and Yokouchi, M. 2008, J. Ceram. Soc. Jpn., 116, 980.
28. Maeda, K., Mito, Y., Yanagase, T., Haraguchi, S., Yamazaki, T. and Suzuki, T. 2007, Chem. Commun., 283.
29. Fink, P. and Datka, J. 1989, J. Chem. Soc. Faraday Trans. 1, 85, 3079.
30. Centeno, M.A., Debois, M. and Grange, P. 1998, J. Phys. Chem. B, 102, 6835.
31. Centeno, M.A., Delsarte, S. and Grange, P. 1999, J. Phys. Chem. B, 103, 7214.

32. Guan, X., Zhang, F., Wu, G. and Guan, N. 2006, Mater. Lett., 60, 3141.
33. Guo, J., Han, A.J., Yu, H., Dong, J.P., He, H.Y. and Long, Y.C. 2006, Micropor. Mesopor. Mater., 94, 166.
34. Dupree, R., Lewis, M.H. and Smith, M.E. 1988, J. Am. Chem. Soc., 110, 1083.
35. van Weeren, R., Leone, E.A., Curran, S., Klein, L.C. and Danforth, S.C. 1994, J. Am. Ceram. Soc., 77, 2677.
36. Impens, N.R.E.N. and Vansant, E.F. 1997, Interface Sci., 5, 95.
37. Hammond, K.D., Dogan, F., Tompsett, G.A., Agarwal, V., Grey, C.P., Conner, W.C. and Auerbach, S.M. 2008, J. Am. Chem. Soc., 130, 14912.
38. van Santen, R.A., van de Graaf, B. and Smit, B. 2001, Stud. Surf. Sci. Catal., 137, 419.
39. Fermann, J.T., Moniz, T., Kiowski, O., McIntire, T.J., Auerbach, S.M., Vreven, T. and Frisch, M.J. 2005, J. Chem. Theor. Comput., 1, 1232.
40. Sierka, M. and Sauer, J. 2001, J. Phys. Chem. B, 105, 1603.
41. Sierka, M. and Sauer, J. 2000, J. Chem. Phys., 112, 6983.
42. Young, D.C. 2001, Computational Chemistry: A Practical Guide for Applying Techniques to Real-World Problems, Wiley, New York, 128.
43. Astala, R., Auerbach, S.M. and Monson, P.A. 2004, J. Phys. Chem. B, 108, 9208.
44. Hill, J.R., Freeman, C.M. and Delley, B. 1999, J. Phys. Chem. A, 103, 3772.
45. Suzuki, K., Noda, T., Sastre, G., Katada, N. and Niwa, M. 2009, J. Phys. Chem. C, 113, 5672.
46. Sillar, K. and Burk, P. 2004, J. Phys. Chem. B, 108, 9893.
47. Smirnov, K.S. and Bougeard, D. 2001, Catal. Today, 70, 243.
48. Bornhauser, P. and Bougeard, D. 2001, J. Phys. Chem. B, 105, 36.
49. Bornhauser, P. and Bougeard, D. 2001, J. Raman Spectros., 32, 279.
50. Kohn, W. and Sham, L.J. 1965, Phys. Rev., 140, A1113.
51. Møller, C. and Plesset, M.S. 1934, Phys. Rev., 46, 618.
52. Gauss, J. 2000, Modern Methods and Algorithms of Quantum Chemistry, J. Grotendorst (Ed.), John von Neumann Institut fuer Computing, 541.
53. Keith, T.A. and Bader, R.F.W. 1993, Chem. Phys. Lett., 210, 223.
54. Kutzelnigg, W. 1980, Isr. J. Chem., 19, 193.
55. Keith, T.A. and Bader, R.F.W. 1992, Chem. Phys. Lett., 194, 1.
56. Ditchfield, R. 1974, Mol. Phys., 27, 789.
57. Wolinski, K., Hinton, J.F. and Pulay, P. 1990, J. Am. Chem. Soc., 112, 8251.
58. Mauri, F., Pfrommer, B.G. and Louie, S.G. 1996, Phys. Rev. Lett., 77, 5300.
59. Charpentier, T., Ispas, S., Profeta, M., Mauri, F. and Pickard, C.J. 2004, J. Phys. Chem. B, 108, 4147.
60. Cheeseman, J.R., Trucks, G.W., Keith, T.A. and Frisch, M.J. 1996, J. Chem. Phys., 104, 5497.
61. Magyarfalvi, G. and Pulay, P. 2003, J. Chem. Phys., 119, 1350.
62. Handy, N.C. and Cohen, A.J. 2001, Mol. Phys., 99, 403.
63. Lee, C., Yang, W. and Parr, R.G. 1988, Phys. Rev. B, 37, 785.
64. Becke, A.D. 1988, Phys. Rev. A, 38, 3098.
65. Miehlich, B., Savin, A., Stoll, H. and Preuss, H. 1989, Chem. Phys. Lett., 157, 200.
66. Sefzik, T.H., Turco, D., Iuliucci, R.J. and Facelli, J.C. 2005, J. Phys. Chem. A, 109, 1180.

67. Vosko, S.H., Wilk, L. and Nusair, M. 1980, Can. J. Phys., 58, 1200.
68. Stephens, P.J., Devlin, F.J., Chabalowski, C.F. and Frisch, M.J. 1994, J. Phys. Chem., 98, 11623.
69. Becke, A.D. 1993, J. Chem. Phys., 98, 5648.
70. Perdew, J.P. 1991, Electronic Structure of Solids, P. Ziesche and H. Eschrig (Eds.), Akademie Verlag, Berlin, 11.
71. Perdew, J.P. and Wang, Y. 1992, Phys. Rev. B, 45, 13244.
72. Becke, A.D. 1996, J. Chem. Phys., 104, 1040.
73. Adamo, C. and Barone, V. 1998, J. Chem. Phys., 108, 664.
74. Zhang, Y., Wu, A., Xu, X. and Yan, Y. 2006, Chem. Phys. Lett., 421, 383.
75. Perdew, J.P., Burke, K. and Ernzerhof, M. 1996, Phys. Rev. Lett., 77, 3865.
76. Perdew, J.P., Burke, K. and Ernzerhof, M. 1997, Phys. Rev. Lett., 78, 1396.
77. Moon, S. and Case, D.A. 2006, J. Comput. Chem., 27, 825.
78. Baldridge, K.K. and Siegel, J.S. 1999, J. Phys. Chem. A, 103, 4038.
79. Hammond, K.D. (unpublished).
80. Gregor, T., Mauri, F. and Car, R. 1999, J. Chem. Phys., 111, 1815.
81. Auer, A.A., Gauss, J. and Stanton, J.F. 2003, J. Chem. Phys., 118, 10407.
82. Wilson, P.J., Amos, R.D. and Handy, N.C. 1999, Mol. Phys., 97, 757.
83. Wilson, P.J., Amos, R.D. and Handy, N.C. 1999, Chem. Phys. Lett., 312, 475.
84. Keal, T.W. and Tozer, D.L. 2003, J. Chem. Phys., 119, 3015.
85. Keal, T.W. and Tozer, D.L. 2004, J. Chem. Phys., 121, 5654.
86. McLean, A.D. and Chandler, G.S. 1980, J. Chem. Phys., 72, 5639.
87. Krishnan, R., Binkley, J.S., Seeger, R. and Pople, J.A. 1980, J. Chem. Phys., 72, 650.
88. Dunning, T.H., Jr. 1989, J. Chem. Phys., 90, 1007.
89. Kendall, R.A., Dunning, T.H., Jr. and Harrison, R.J. 1992, J. Chem. Phys., 96, 6796.
90. Woon, D.E. and Dunning, T.H., Jr. 1993, J. Chem. Phys., 98, 1358.
91. Peterson, K.A., Woon, D.E. and Dunning, T.H., Jr. 1994, J. Chem. Phys., 100, 7410.
92. Davidson, E.R. 1996, Chem. Phys. Lett., 260, 514.
93. Pacific Northwest National Laboratory, EMSL Basis Set Exchange, https://bse.pnl.gov/bse/portal.
94. Turaga, S.C. and Auerbach, S.M. 2003, J. Chem. Phys., 118, 6512.
95. Dapprich, S., Komáromi, I., Byun, K.S., Morokuma, K. and Frisch, M.J. 1999, J. Mol. Struct. THEOCHEM, 461-462, 1.
96. Scott, A.P. and Radom, L. 1996, J. Phys. Chem., 100, 16502.
97. Andrade, S.G., Gonçalves, L.C.S. and Jorge, F.E. 2008, J. Mol. Struct. THEOCHEM, 864, 20.
98. Yamaguchi, Y., Frisch, M.J., Gaw, J., Schaefer, I., H.F. and Binkley, J.S. 1986, J. Chem. Phys., 84, 2262.
99. Frisch, M.J., Yamaguchi, Y., Gaw, J.F., Schaefer, I., H.F. and Binkley, J.S. 1986, J. Chem. Phys., 84, 531.
100. Bussemer, B., Schröder, K.P. and Sauer, J. 1997, Solid State Nucl. Magn. Reson., 9, 155.

101. Bull, L.M., Bussemer, B., Anupõld, T., Reinhold, A., Samoson, A., Sauer, J., Cheetham, A.K. and Dupree, R. 2000, J. Am. Chem. Soc., 122, 4948.
102. Loewenstein, W. 1954, Am. Mineral., 39, 92.
103. Melchior, M.T., Vaughan, D.E.W. and Jacobson, A.J. 1982, J. Am. Chem. Soc., 104, 4859.
104. Melchior, M.T., Vaughan, D.E.W. and Pictroski, C.F. 1995, J. Phys. Chem., 99, 6128.
105. Vega, A.J. 1996, J. Phys. Chem., 100, 833.
106. Valerio, G. and Goursot, A. 1999, J. Phys. Chem. B, 103, 51.
107. Casanovas, J., Ilas, F. and Pacchioni, G. 2000, Chem. Phys. Lett., 326, 523.
108. Mägi, M., Lippmaa, E., Samoson, A., Engelhardt, G. and Grimmer, A.R. 1984, J. Phys. Chem., 88, 1518.
109. Makulski, W., Jackowski, K., Antušek, A. and Jaszuński, M. 2006, J. Phys. Chem. A, 110, 11462.
110. Wasylishen, R.E. and Bryce, D.L. 2002, J. Chem. Phys., 117, 10061.
111. Chauvel, J.P. and True, N.S. 1985, Chem. Phys., 95, 435.
112. Sauer, J., Eichler, U., Meier, U., Schäfer, A., von Arnim, M. and Ahlrichs, R. 1999, Chem. Phys. Lett., 308, 147.
113. Jameson, C.J., Jameson, K.A., Oppusunggu, D., Wille, S., Burrell, P.M. and Mason, J. 1981, J. Chem. Phys., 74, 81.
114. Barthomeuf, D. 2003, Micropor. Mesopor. Mater., 66, 1.
115. Corma, A., Viruela, P. and Fernández, L. 1998, J. Mol. Catal. A Chem., 133, 241.
116. Fleischer, H., McKean, D.C. and Torto, I. 2002, Spectrochim. Acta A Mol. Biomol. Spectros., 58, 911.
117. Fleischer, H., McKean, D.C., Torto, I. and Boggs, J.E. 2002, J. Mol. Struct., 604, 221.
118. Márquez, A., Fernández Sanz, J. and Odriozola, J.A. 2000, J. Non-Cryst. Solids, 263,
119. Yamamoto, K., Sakata, Y., Nohara, Y., Takahashi, Y. and Tatsumi, T. 2003, Science, 300, 470.
120. Astala, R. and Auerbach, S.M. 2004, J. Am. Chem. Soc., 126, 1843.
121. Lesthaeghe, D., Van Speybroeck, V. and Waroquier, M. 2004, J. Am. Chem. Soc., 126, 9162.
122. Lesthaeghe, D., Van Speybroeck, V., Marin, G.B. and Waroquier, M. 2005, J. Phys. Chem. B, 109, 7952.
123. Zheng, A., Wang, L., Chen, L., Yue, Y., Ye, C., Lu, X. and Deng, F. 2007, ChemPhysChem, 8, 231.
124. Svensson, M., Humbel, S., Froese, R.D.J., Matsubara, T., Sieber, S. and Morokuma, K. 1996, J. Phys. Chem., 100, 19357.
125. Wu, G., Yang, Y., Wang, G., Zhang, F. and Guan, N. 2008, Chin. J. Catal., 29, 203.
126. van Koningsveld, H., van Bekkum, H. and Jansen, J.C. 1987, Acta Crystallogr., B43, 127.
127. Lonsinger, S.L., Chakraborty, A.K., Theodorou, D.N. and Bell, A.T. 1991, Catal. Lett., 11, 209.